JOURNAL OF Materials CHEMISTRY

Preparation of titania mesoporous materials using a surfactant-mediated sol–gel method†

P. Kluson,*[a] P. Kacer,[a] T. Cajthaml[b] and M. Kalaji[c]

[a]*Faculty of Chemical Technology, ICT Prague, Technicka 5, 166 28 Prague, Czech Republic. E-mail: kluson@ic.ac.uk*
[b]*Institute of Microbiology, Academy of Sciences of the Czech Republic, Videnska 1083, 142 20 Prague, Czech Republic*
[c]*Department of Chemistry, University of Wales in Bangor, Gwynedd, UK LL57 2UW*

Received 14th June 2000, Accepted 13th September 2000
First published as an Advance Article on the web 5th January 2001

Small titania particles were generated within the template of a non-ionic surfactant (TX-100) reverse micelle assembly by the sol–gel method from titanium(IV) isopropoxide. Cyclohexane was used as the reaction solvent to form a reverse micelle system with a low water to surfactant ratio. Gelling, *i.e.*, hydrolysis and polycondensation, were observed by means of viscosity measurements. The transparent raw gels obtained were dried under vacuum at 372 K. The dry gels were then either thermally decomposed directly to TiO_2 or the organic content (surfactant) was substantially reduced first by supercritical fluid extraction with CO_2 and then thermally treated. Special attention was paid to the effect of temperature on the extent of crystallisation of individual crystallographic phases of TiO_2. Gels, partly decomposed gels and gels after the supercritical fluid extraction were investigated by XRD, XPS, IR, TPR, thermogravimetry, mass spectrometry, elemental analysis, UV–vis, SEM and extensive gas adsorption measurements. Their properties were related to the structure and other features of the final nanosized TiO_2 particles. The anatase form of TiO_2 with a very high specific surface area and well-developed mesoporous and microporous structure was prepared.

Introduction

Metal oxide particles prepared by a sol–gel technique usually exhibit phase, size and structure uniformity.[1–3] The most common variation is associated with hydrolysis of metal alkoxides.[4,5] An initial liquid alkoxide is transformed (by hydrolysis and polycondensation) to the gel which is a polymeric structure incorporating cross linked –O–metal–O– chains.[1,6,7] The quality of the gel and consequently the quality of the monomeric oxide strongly depend on the arrangement (kinetics) of the hydrolysis step. The step involving the removal of organic molecules from the gel should also significantly affect the final structure and its surface properties.

When titanium(IV) oxide is involved as the desired structure, many possible applications might be taken into account depending on the properties (transparency, photoactivity, *etc.*) and the microstructure (surface area, pore size distribution, particle size, crystallographic structure) of the product. The sol–gel transformation has a capacity to yield the TiO_2 material with an unusually high surface area, small nanoparticles uniform in size and shape and with narrow pore size distribution. When deposited on glass or quartz, TiO_2 layers of a thickness from a few nm to 1 micron with very good transparency have been obtained.[8,9] Many of the possible applications arise from the semiconductor nature of titania and the photoactivity of anatase.[10–13] When the TiO_2 particle absorbs a photon (typically with a wavelength less than $\lambda = 365$ nm) an electron is transferred from the semiconductor valence band[14] to the conduction band. It functions there as a reducing agent, which leaves an electronic vacancy behind that is oxidising.[6,14] Titania precursor gels, or their reduced forms, are mostly used as ultrathin film coatings, nanostructured membranes, fibres, photoactive catalytic nanoparticles, *etc.*, in fuel cells, as electrodes in electrochemistry and electrocatalysis, in microoptics and electrooptics and in photocatalysis.[1,5,6,8–35]

The most commonly used alkoxide for the sol–gel preparation[1] of TiO_2 particles is titanium(IV) isopropoxide (TIOP). However, as with other transition metal alkoxides, it hydrolyses rapidly and precipitates.[1,28] Hydrolysis and polycondensation start immediately in the presence of water[1,6,36] (even when in contact with atmospheric moisture[37]). Since the precipitated particles are usually quite large and their structure inhomogeneous it is desirable to slow down this process as much as possible.[1,9]

Compared to other methods[8,15,24,27,38–40] the surfactant-mediated sol–gel[1,9,36,41] provides a good control of the hydrolysis rate. Titanium alkoxide is solubilised in reverse micelles to hydrolyse with the limited amount of water contained inside the micelle. Then gelling (*i.e.* hydrolysis and polycondensation = polymerisation → –O–Ti–O–Ti– network) depends mostly on the structure of the surfactant organising itself around the resultant polar TiO_2 particles.[1,9] Depending on the surfactant structure, differently shaped and sized particles are obtained ranging from uniform monodispersed spheres to long particles with a high degree of orientation (*e.g.* a lamellar structure).[1,42] The rate of hydrolysis can be also controlled through the surfactant's structure-dependent water content.

In this work we report on the *in situ* sol–gel generation of titania nanoparticles within templates of surfactant assemblies (reverse micelles).[43] Attention was paid to alternative methods for the removal of the organic content from the gel. Thermal decomposition, in this work arranged as a temperature

†Electronic supplementary information (ESI) available: comments on gel preparation and high resolution N_2 adsorption and desorption isotherms at 77 K on the surface of SFE (mode-3) gel. See http://www.rsc.org/suppdata/jm/b0/b004760k/

 DOI: 10.1039/b004760k

programmed reduction, has been universally applied[1,9,36,41,42] in the past. However, there are important general limitations such as the undesirable extent of crystallisation at temperatures[13,20,22,23,38,39] at which the surfactant could not be completely decomposed (lower specific surface area, *etc.*). In this context we tested the supercritical fluid extraction as an alternative.[44–46] Supercritical fluids (SFs) are interesting physico-chemical systems.[47] Some of their properties such as total miscibility with permanent gases and diffusion coefficients resemble those of gases, whilst their density can be such that they can solubilise a wide variety of substrates.[44–52] CO_2 is the most studied SF and can be easily obtained (critical point of CO_2—7.4 MPa and 304 K). Furthermore, it is environmentally more friendly than the traditionally used organic extraction solvents.[47–49] After the supercritical fluid extraction, gels were thoroughly investigated and their properties compared with the materials obtained by the thermal treatment of the original raw gels. Special attention was paid to optimising the conditions under which the photoactive anatase is formed with respect to the extent of the specific surface area and its microstructure.

Experimental

Preparation of a gel

Reverse micelles of Triton X-100 (Aldrich, 99.99%) in cyclohexane were used for the preparation of the gels[43] (Aldrich, HPLC grade, water content less than 0.01%). Triton X-100 (TX-100) is a well-defined non-ionic surfactant.[53–57] Its structure contains a long hydrophilic poly(oxyethylene) chain terminated with a hydroxyl group (Fig. 1). A constant molar ratio of water to surfactant $R=1$ was used in this work. Zhu *et al.*[43,58] have shown that up to a value of $R\sim1$, water molecules are predominantly associated with the terminal hydroxyl group of the TX-100 and that water molecules do not significantly compete with cyclohexane in the solvation of most of the chain oxyethylene groups.[43] Triton X-100 does not form spherical micelles and thus its hydrodynamic diameter calculated for the spherical particles by means of the Stokes–Einstein equation[43,58] could only be referred to as an apparent diameter. For the composition used in this work, (TX-100/cyclohexane = 0.85 mol kg^{-1}) the hydrodynamic diameter used was that calculated by Zhu *et al.*[43] to be $D_h\sim61.0$ nm at $R=1$ (at 303 K) with an aggregation number of about 40. In the preparation millipore water was used. The alkoxide used was titanium(IV) isopropoxide (TIOP) (Aldrich, 99.99%).

Process of gelling

The process of gelling was followed by using a Eurostar ViscController module (Ikka) at 303 K. Throughout this work, the viscosity of a mixture of TX-100/cyclohexane/water before the addition of TIOP was assumed as an initial value and referred to as zero. The viscosity at the point of visual gelling completion was taken as one.

Temperature programmed reduction (TPR)

Fresh gels were exposed to air at 293 K for 24 h (ageing) and then dried in a rotating vacuum evaporator at 372 K for 4 h. Afterwards they were placed in a quartz tube inside the TPR apparatus and decomposed either in air or oxygen (flow rate, $Q=100$ cm^3 min^{-1}) at ten different isothermal levels within the temperature range 473 to 1123 K. Each temperature elevation was attained at a constant heating rate of 20 °C min^{-1}.

Supercritical fluid extraction and elemental analysis

To improve the effectiveness of this step the pressurised fluid extraction (PFE) preceded the supercritical fluid extraction step. The apparatus was assembled from Perkin-Elmer 200 LC pump, oven (Waters) and a needle valve (Altech) as a back pressure regulator. The extraction was carried out at a working pressure of 14.2 MPa and at 373 K for 60 min. Methanol (HPLC grade, Fluka, water content less than 0.002%) was used as an extraction solvent with a flow rate of 1 ml min^{-1}. During this initial step a sample was placed in a supercritical fluid extraction cell (Suprex).

Supercritical fluid extraction (SFE) was performed in a supercritical fluid extractor (Suprex) equipped with a PrepMaster module (modifier pump) and an AccuTrap module (VaryFlow restrictor). Carbon dioxide SFE grade (Messer Griesheim) was used as the extraction fluid and HPLC grade methanol as a modifier.[45–47] The working pressure of this step was 45.6 MPa and the flow rate was kept constant at 1 ml min^{-1}. The SFE procedure was typically started by pressurising the cell with a mixture of carbon dioxide with 10% methanol for 60 min at 373 K (45.6 MPa). Then a dynamic step

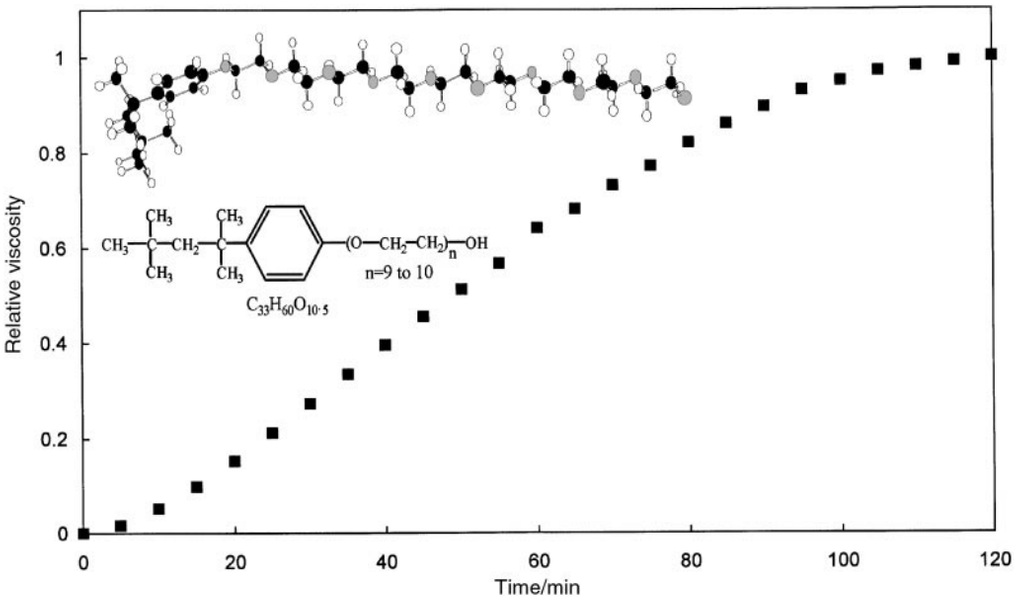

Fig. 1 The viscosity curve of gelling shown together with a formula and a 3D model of a molecule of the TX-100 surfactant. The initial viscosity of a mixture of TX-100/cyclohexane/water (before addition of TIOP) was set to zero, the viscosity at the point of visual gelling completion was taken as one.

with pure carbon dioxide followed at the same conditions. This step was carried out for 60 min (mode-1), 120 min (mode-2) or 180 min (mode-3).

Dried gels (372 K) and gels after the SFE were analysed for their carbon content using elemental analysis (CHN-240C, Perkin-Elmer). The amount of CO_2 evolved was determined both gravimetrically and spectroscopically. The conditions[47] of the PFE and SFE steps were optimised in a number of experiments with the aim of minimising the organic carbon content and maximising the surface area.

Thermogravimetric analysis (TGA)

The effect of temperature on gels after the SFE process was studied using TGA (TG 750, Stanton and Redcroft) with samples positioned in a platinum holder. The rate of temperature rise was $20\,^{\circ}C\,min^{-1}$ in air ($10\,ml\,min^{-1}$). Gaseous products of the decomposition were analysed using a GC–MS analytical system (Saturn 2000, Varian) equipped with an ion trap mass analyser, MS–MS mode and a chemical ionisation module (methanol). The GC column was ultra DB-5 ($60\,m \times 0.25\,mm \times 0.25\,\mu m$). Solid fractions remaining in the furnace at each temperature level were extracted in toluene for further analysis.

X-Ray powder diffraction analysis (XRD)

XRD (R. Seifert Co.) was employed to examine the crystallographic phase structure of the TiO_2 samples and crystallite size using Bragg–Brentano focusing geometry, Co-Kα radiation and a graphite monochromator. Interplanar spacings and intensities were compared with the PDF 2 data base.[59] Crystallite size was computed from the Scherrer equation.

Infrared spectroscopy

Samples of dry gels (372 K), gels after the supercritical fluid extraction, partially decomposed gels and various final titania samples were analysed using IR spectroscopy. The spectra were recorded using a Nicolet 740 spectrometer.

XPS analysis

XPS analysis of gels after the supercritical fluid extraction was carried out using an ESCA 310 spectrometer (Gammadata Scientia AB) with a rotating anode, monochromator and a hemispheric analyser of electrons in a high vacuum (10^{-9} mbar). An Al-Kα source of radiation ($h\nu = 1486.6$ eV) was used for the excitation of electrons.

Adsorption isotherms of CO_2 and N_2, PSD and BET analysis

Volumetric adsorption experiments with nitrogen were conducted using an Omnisorp 100 (Coulter) at 77 K in a static regime and a gravimetric sorption analyser IGA 002 (Hiden). Each sample was placed under high vacuum (10^{-5} Torr) before measurements (423 K for 6 h). Adsorption experiments with carbon dioxide at 298 K were performed using a Sorptomatic 1800 (Carlo Erba).

UV–vis absorption spectroscopy

Ultraviolet–visible spectroscopy measurements (Lambda 19, Perkin-Elmer, absorption mode) were carried out with the aim of assessing the presence of quantum size effects,[3,39,60–62] location of absorption edges of anatase–rutile and anatase, and to support the suggested initial gel structure and the gel structure after the supercritical fluid extraction. Dry samples were dispersed in water and mixed by sonification.

SEM

Micrographs of fresh gels dried at 372 K, gels decomposed at various temperatures and gels after the supercritical fluid extraction were recorded using an SEM apparatus (Hitachi S-520 at $U = 14$ kV). Samples were fixed on a microscopy holder by a conductive carbon tape and sputtered with gold in plasma.

Results and discussion

Reverse micelle solutions (TX-100/cyclohexane/water) were slightly turbid before adding TIOP at 303 K. However, upon the addition of the alkoxide, the solutions became clear and remained transparent up to the point of visual gelling completion. The presence of a white precipitate, usually ascribed[1,6,7,9,11,22,31,33] to the appearance of $Ti(OH)_4$ formed by total hydrolysis of the initial alkoxide, was not observed in any of the experiments. This supports the notion that the most prominent products of the hydrolysis step are the reaction (gelling) intermediates coordinating Ti with one or two (or three) OH groups and three or two (or one) isopropoxide parts in their molecules, respectively.[6] These intermediates are very unstable and react immediately upon their formation in parallel with the progress of the hydrolysis step giving an initial polymeric structure. As this step proceeds and the structure evolves the transparent gel is obtained. The viscosity curve shown in Fig. 1 typically started with a short induction period most likely corresponding to the transport of the alkoxide into the core of the reverse micelle and to the formation of enough intermediate molecules for initiation of the polycondensation. Under these conditions gelling was completed in about 110 min. The raw gel was allowed to stay open to the air for 24 h and then dried under vacuum at 372 K. Some aspects of the hydrolysis and condensation steps are also discussed in the IR section. Further investigations on structural changes occurring during this initial step, based on *in situ* NMR hydrolysis simulation, are now in progress and will be reported in a further communication.

Gels dried at 372 K in a vacuum were treated either thermally (TT) or by supercritical fluid extraction (SFE) followed by thermal treatment (SFE-T). Both sets of samples were analysed for their carbon content. For the first set (TT) and for samples treated thermally after the SFE (SFE-T) it was found that temperatures of 823 and 923 K, respectively, were necessary to totally complete the decomposition of the organic component.

Elemental analysis showed that the carbon content of the gels dried at 372 K was 59 wt%. Upon treatment of such gels with SFE, a dry material (aerogel) with still a relatively high carbon content was obtained. The highest level was 18.5 wt% after the SFE mode-1 whereas the lowest one achieved was 9.8 wt% (mode-3). Mode-2 led to a gel with a carbon content of 11.8 wt%. Further prolongation of this step had only little effect on the carbon content.

Raw solid gels dried at 372 K did not show any indication of the presence of any crystallographic forms of TiO_2 (X-ray diffraction). As the temperature inside the TPR furnace was raised, anatase and later rutile started to slowly appear. At 523 K the typical XRD pattern showed no peaks. It was not until a temperature of 623 K was reached that the first significant peak of anatase at $2\theta = 25.4^{\circ}$ was identified (the peak at about $2\theta = 5^{\circ}$ is characteristic of instrumentation). At 723 K, the temperature was high enough (Fig. 2) for the formation of all the major diffraction peaks of anatase. As the temperature was further increased diffuse bands, initially formed at 723 K, became sharper and more intense. Above 923 K diffraction lines for rutile also appeared. Samples of the gels treated by supercritical fluid extraction (=amorphous) and subsequently thermally decomposed were more resistant to the crystallisation than those only calcined in oxygen. First peaks became

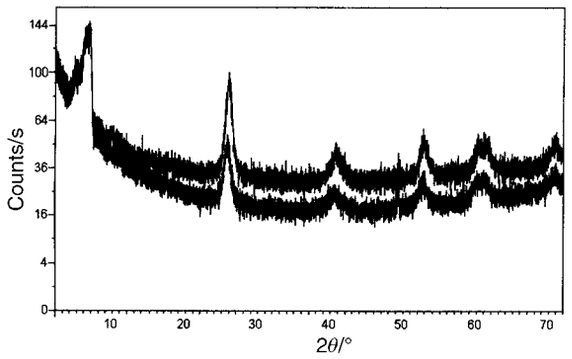

Fig. 2 Diffuse XRD patterns of anatase formed from the sample treated only thermally at 723 K (upper spectrum), and treated at 773 K from the SFE (mode-3) gel (lower spectrum).

evident at 773 K and were even more diffuse than those of the sample treated only thermally at 723 K (Fig. 2). Below this level all samples after supercritical fluid extraction were amorphous (pseudo-amorphous).

From the width of the diffraction peaks and the Scherrer equation the crystallite size of titania was calculated. The mixed anatase–rutile sample prepared at 1123 K from the dry gel exhibited the largest particles ($D=11.3$ nm); the smallest particles of this group (TT) were evaluated for the sample decomposed at 723 K (4.6 nm). SFE-T samples possessed the minimum crystallite size at 773 K with a value of $D=3.8$ nm.

Surface areas of the titania samples treated only thermally (TT) increased from 487 ± 3 m^2 g^{-1} at 473 K up to 679 ± 5 m^2 g^{-1} at 723 K. As the fraction of amorphous titania decreased with increasing temperature, S_{BET} also decreased and at 1123 K it only reached 187 ± 3 m^2 g^{-1}. The very striking feature of the gel samples after SFE was their nearly constant surface area, which was also independent of the mode of the SFE. The S_{BET} values varied from 619 ± 5 m^2 g^{-1} (mode-1) to 628 ± 5 m^2 g^{-1} (mode-3). In this set of samples (again for mode-3) the thermal treatment (SFE-T) at a temperature of 773 K resulted in the highest achieved surface area, $S_{BET}=781$ m^2 g^{-1}. In comparison, the surface area for the thermally treated sample at 723 K peaked at 679 m^2 g^{-1}; the surface area of the corresponding SFE-T sample was $S_{BET}=752$ m^2 g^{-1}. These results are summarised in Table 1.

Fig. 3(a) shows the high-resolution nitrogen adsorption–desorption isotherm at the surface of the SFE gel (mode-3) at 77 K. The x-axis (pressure) is plotted on a logarithmic scale to highlight the low-pressure region up to the relative pressure of $P/P_0=1$. Relatively significant uptake of nitrogen inside of a very low-pressure region indicates contribution of narrow micropores (less than $r=1$ nm) which is not a common feature of titania materials. Above this region there is a zone in the middle of which a point of inflection is located. This part corresponds to the saturation of edges and other inhomogeneous sites on the surface and precedes monolayer formation. The clear indication of this monolayer is located around $P/P_0=0.0006$. The adsorption capacity of the completed layer, if it is plotted on a linear scale, is about 130 cm^3 g^{-1} at the relative pressure of $P/P_0=0.08$. The most significant part of the carbon dioxide adsorption isotherm at 298 K on the same surface is shown in Fig. 3(b).

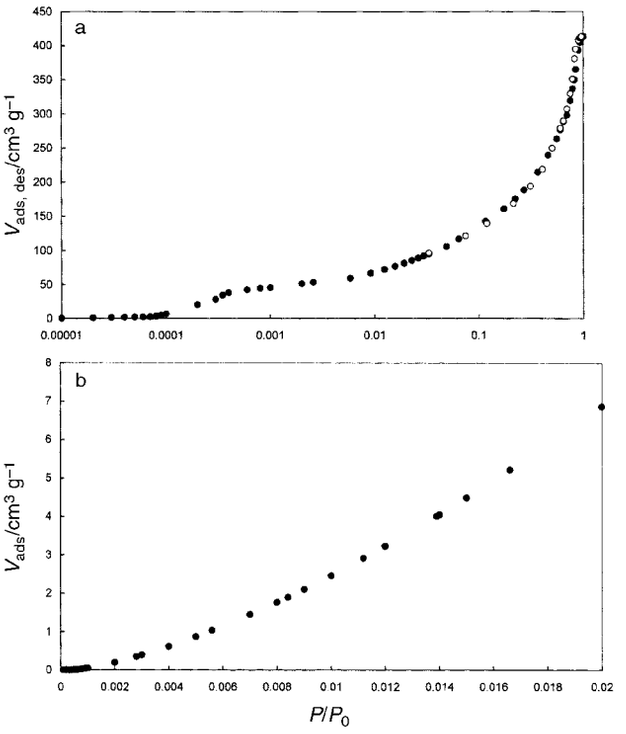

Fig. 3 (a) High-resolution adsorption (●) and desorption (○) isotherms of N_2 at 77 K on the surface of SFE (mode-3) gel plotted with a logarithmic scale of the pressure axis. (b) The most significant part of the CO_2 adsorption isotherm at 298 K onto the same surface for the DR analysis.

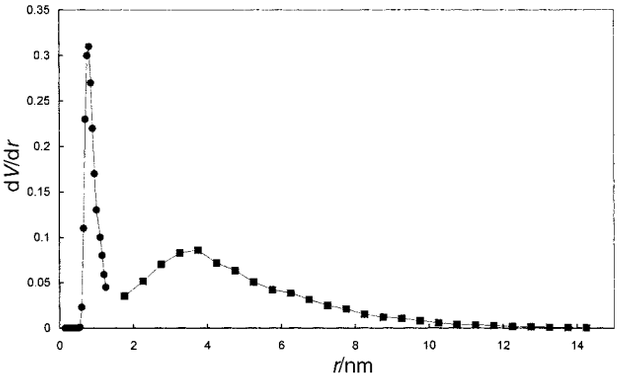

Fig. 4 Mesopore (■) and micropore (●) size distribution patterns of the SFE (mode-3) gel.

Mesopore size distribution pattern of the SFE mode-3 gel evaluated from the desorption branch of the N_2 isotherm by the BJH method[63] is shown in Fig. 4. Unimodal distribution covers

Table 1 Some characteristic features of the thermally treated only gels (TT), gels after SFE and SFE-T samples (am/p-am = amorphous/pseudo-amorphous; an = anatase; rut = rutile)

Sample	Crystallographic phase	Temperature/K	Crystallite size/nm	S_{BET}/m^2 g^{-1}	S_{meso}/m^2 g^{-1}	S_{micro}/m^2 g^{-1}	S_{total}/m^2 g^{-1}
TT	am/p-am	473		487			
TT	an	723	4.6	679	426	273	699
TT	an-rut	1123	11.3	187			
SFE (mode-1)	am/p-am			619			
SFE (mode-2)	am/p-am			623			
SFE (mode-3)	am/p-am			628	461	180	641
SFE-T (mode-3)	an	773	3.8	781	495	315	810
SFE-T (mode-3)	an	723	4.1	752	488	289	777

the area from 1.3 nm up to 14.3 nm peaking at approximately $r = 3.8$ nm. Owing to the steep initial increase in the dV/dr value the most significant interval is located between $r = 1.5$ and 4 nm. This pattern corresponds to the predominantly mesoporous character of the gel. Based on the assumption of a cylindrical pore geometry, the geometrical surface of the mesoporous region area was evaluated and attained a value of $S_{meso} = 461\ m^2\ g^{-1}$. The contribution of the microporous region to the overall volume was determined from the CO_2 isotherm by the DR (DRS) method[64–67] and is also given in Fig. 4. It starts just below $r = 0.6$ nm, having its quite sharp maximum at $r = 0.8$ nm and then decaying with an increasing pore size. The corresponding S_{micro}, assuming only contribution of the pores inside of the interval 0.4–1.3 nm, was $180\ m^2\ g^{-1}$. Thus the overall geometrical surface area of the gel was $S_{total} = 641\ m^2\ g^{-1}$. It is a value nearly identical to that determined by the BET method ($628\ m^2\ g^{-1}$). The SFE-T (mode-3) sample treated thermally at 773 K (already with the anatase structure) with an $S_{BET} = 781\ m^2\ g^{-1}$ did not significantly differ in the contribution of its mesostructure from the original SFE gel. The increase of $S_{total} = 810\ m^2\ g^{-1}$ was mainly due to more significant contribution of the micropore region. At this temperature, the organic carbon content is already negligible and a selective blocking of very narrow pores with the surfactant or its decomposition products is not possible. The mesoporous phase of the original gel is not apparently as sensitive to the presence of larger molecules as the microporous one (summarised in Table 1).

The transformation of the gels was also examined by using infrared spectroscopy. Fig. 5(A) shows a typical spectrum of the surfactant TX-100. The spectrum is characterised by the presence of strong absorbances associated with the symmetric and asymmetric vibrations of the alkyl chains at 2920 and 2850 cm^{-1}, respectively. Furthermore, the presence of the ether linkage is manifested by the strong absorbance centred around 1150 cm^{-1}. The presence of the surfactant is still evident in the spectrum of the raw gel that was dried at 372 K [Fig. 5(B)]. Indeed the two spectra [Figs. 5(A) and 5(B)] are very similar except for the increased intensity of the OH group whose origin is likely to be occluded water and ≡Ti–OH groups. The presence of water is supported by the appearance of the bending mode of water (δH_2O) at 1648 cm^{-1} which, as expected, is not present in the spectrum of the surfactant. Fig. 5(C) shows the striking effect upon the SFE treatment of the raw gel. The presence of Ti–O groups, either from titanium dioxide or the –Ti–O–Ti–O– polymeric network, is unequivocally demonstrated by the presence of the strong, but broad absorbance between 500 and 900 cm^{-1}. Furthermore, the ratio of the intensities of the OH bending and stretching modes relative to those bands originating from the surfactant is greatly enhanced compared to the thermally treated sample. Upon thermal treatment of the SFE gels the original structure of the TX-100 slowly disappears. At 473 K as well as at 573 K all the major bands of the surfactant are still evident. However, at 673 K the IR spectrum already resembles a typical curve of bulk titanium dioxide, which is even more evident at 773 K. Despite the fact that the band at 1648 cm^{-1} is less intensive at higher temperatures, the lasting presence of the OH stretching mode bears upon a high degree of surface hydroxylation. This is advantageous due to the known fact[4,6,11–15,25,35,36] that surface OH groups have a positive effect on the photocatalytic activity of anatase (high capacity for oxygen adsorption).

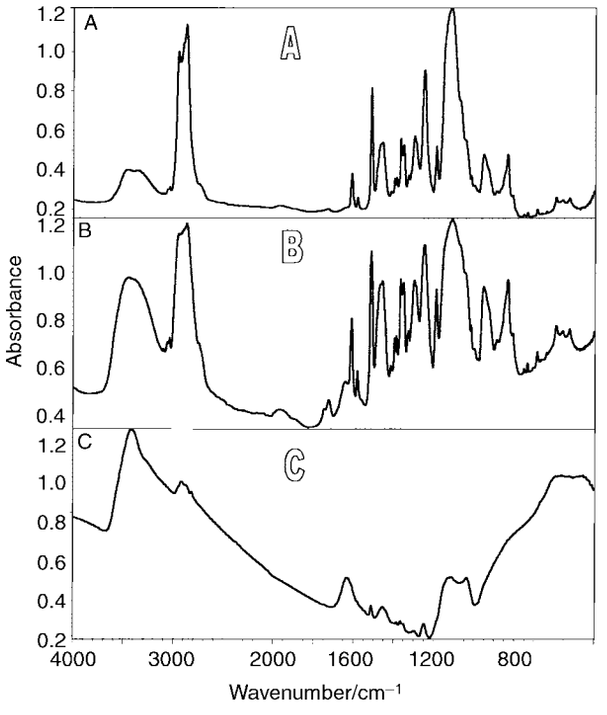

Fig. 5 IR spectra of pure TX-100 (A), a typical raw gel formed in a reverse micelle system and dried at 372 K (B) and of a gel after SFE (C).

The mechanism of the surfactant decomposition can be addressed by considering the long poly(oxyethylene) chain of the surfactant, which is a part of the molecule where oxygen attacks first.[6] This results in partial or complete oxidation of the hydrophilic part of the chain. Such a step yields small and volatile molecules, which evaporate quickly upon their formation and hence could not be detected in the isolated material. Relatively high temperatures are needed to decompose the more resistant hydrophobic part of the molecule and to complete the removal of the organic content.

Some of the conclusions drawn from the IR results were confirmed by TGA and mass spectrometry. The TGA curve of a typical SFE gel is given in Fig. 6. The very beginning part of the curve is rather steep. It resembles that of water molecules physisorbed on the surface.[4,6,11–15,25,35,36] This process is limited to temperatures below 413 K. Initial attack of the least resistant part of the surfactant molecule to oxidation (the hydrophilic chain) starts[6] at about the same temperature (423 K) and is indicated by a change in the slope and in the formation of a "bump".

Separate experiments with the SFE gel in a TPR furnace connected to a GC-ion trap analyser with a chemical source of ionisation (CI) revealed two principal molecular peaks with equal masses of 44 which are due to carbon dioxide, the product of complete oxidation, and acetaldehyde—an expected intermediate. A third molecular peak with a mass of 48 also appeared later; however, its origin is still unknown. This part of the decomposition process terminated just below 623 K. Above this temperature level there was no indication of the existence of the residual parts of the decomposed or partly decomposed

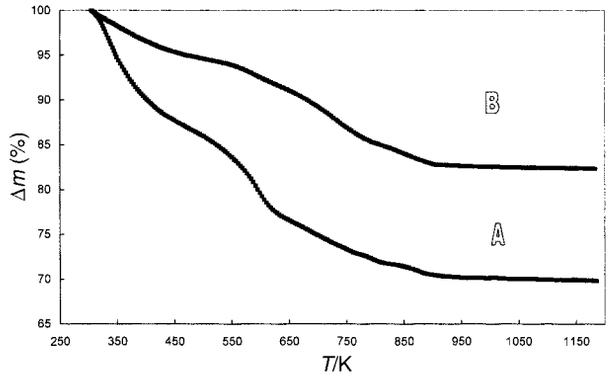

Fig. 6 TGA curves of a typical SFE gel (A) and of the SFE gel treated first in the TPR furnace at 623 K (B).

poly(oxyethylene) chain. Furthermore, the formation of molecules, except carbon dioxide, with the above mentioned molecular masses ceased. Analysis of the solid content of the TPR furnace that was extracted in toluene showed the presence of a molecular fragment with a mass of 205 or 206 as the prevailing component at 623 K. At 823 K the process of decomposition is completed and the organic carbon content is practically zero. The mechanism of this step is not entirely clear yet and it is being intensively investigated. It seems that at least a part of this fragment is temporarily stabilised through the formation of a quinone structure.

Differences among two arbitrarily chosen stages of the SFE gel thermal decomposition were also studied. The first sample was treated thermally at 473 K in the TPR furnace and then analysed by TGA. Its curve still resembled that of the original gel given in Fig. 6. The second sample was treated at 623 K—the temperature level at which the presence of the hydrophilic part of the molecule has already been significantly lowered. Its TGA curve is quite flat at low temperatures, more significant weight loss could be observed above this temperature corresponding to the oxidation of hydrophilic residues and initial oxidation of the hydrophobic part (curve B shown in Fig. 6). When the original sample was treated at 723 K the total weight lost was less then 10%, concentrated in the upper temperature region (above 723 K).

XPS analysis represents a valuable insight into the surface structure of SFE gels. From the general XPS electron spectrum shown in Fig. 7(a) and measured within a range of binding energies of 0–1000 eV, the data imply that surface and subsurface layers (5 nm deep) of the typical SFE gel sample (mode-3) contain only the expected elements: titanium, oxygen and carbon. Spectra of individual lines of Ti 2p, O 1s and C 1s measured at high resolution show [Fig. 7(b)–(d)] that oxygen and carbon are present in three chemically non-equivalent states. From their integral intensities the calculated surface composition is as follows: $Ti_{1.00}O^{\alpha}_{2.05}O^{\beta}_{0.78}O^{\gamma}_{0.43}C^{\alpha}_{1.38}C^{\beta}_{1.55}C^{\gamma}_{0.10}$ with an experimental error of $\pm 10\%$. In this summary formula individual chemical states of oxygen and carbon are given according to the sequence of increasing binding energies of 1s electrons. This formula also reflects the fact that the information depth of the ESCA method is only ~ 5 nm. The overall abundance of carbon on the surface is significantly higher than the average volume concentration of carbon in the SFE gel ($\sim 9.8\%$) found by elemental analysis. It points to a preferential surface location of the surfactant, which tends to organise itself around forming TiO_2 polar particles and their precursors in the SFE gel. Values of binding energies of individual components and their possible interpretations were obtained on comparison of these values with published data for various chemical states. Higher surface occurrence of the C 1s (α) assigned to the existence of the CH_x, C–C (hydrocarbons) could be ascribed to the geometrical orientation of the hydrophobic part of a surfactant molecule during gelling. Other spectral components also reflect the known structure of TX-100 or strong surface hydroxylation. XPS also pointed out that values of the binding energies (for the Ti 2p line the measured value of the binding energy of $E_B = 458.6$ eV was obtained) and the Ti 2p spectrum structure are identical to those of anatase! This is quite an unexpected result. However, it could be assumed as evidence that within the structure of the SFE-only treated gel the tetrahedral form of TiO_2 already exists or that the –O–Ti–O–Ti– network is already organised into the anatase-identical structure.

UV–vis (absorption mode) profiles of raw gels and gels after the SFE are similar. The sharp increase in absorbance in the UV region starts at about 400 nm and peaks at 375 nm. The absorption spectrum of the anatase–rutile mixture formed at 1123 K has a maximum at about 385 nm and for the well-crystallised anatase sample (923 K) the absorption edge was blue-shifted toward a value of 365 nm. None of the data pointed to the presence of small particle quantum size effects.

A flat, homogeneous surface and few surface defects are characteristic features of a raw gel dried at 372 K as shown in Fig. 8. These properties are of fundamental importance when reaction mixtures in the early stages of gelling are used as

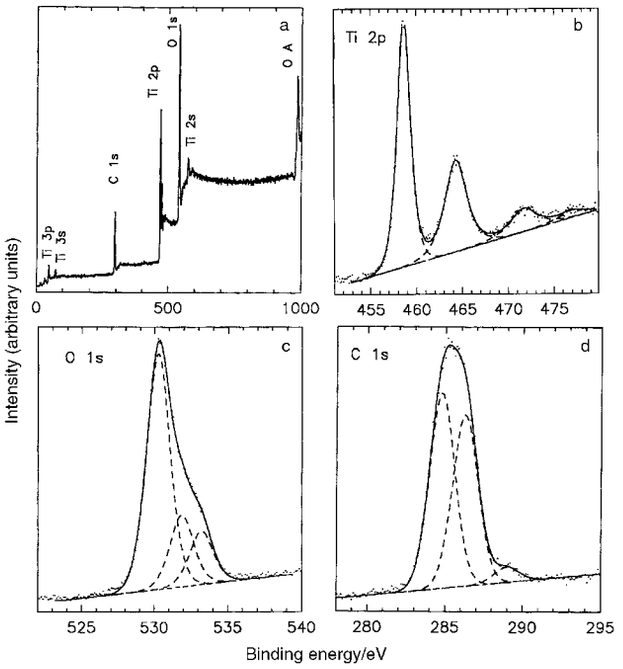

Fig. 7 (a) XPS electron spectrum measured with a sample of the SFE (mode-3) gel. (b)–(d) XPS spectra of individual lines of Ti 2p, O 1s and C 1s measured at high resolution.

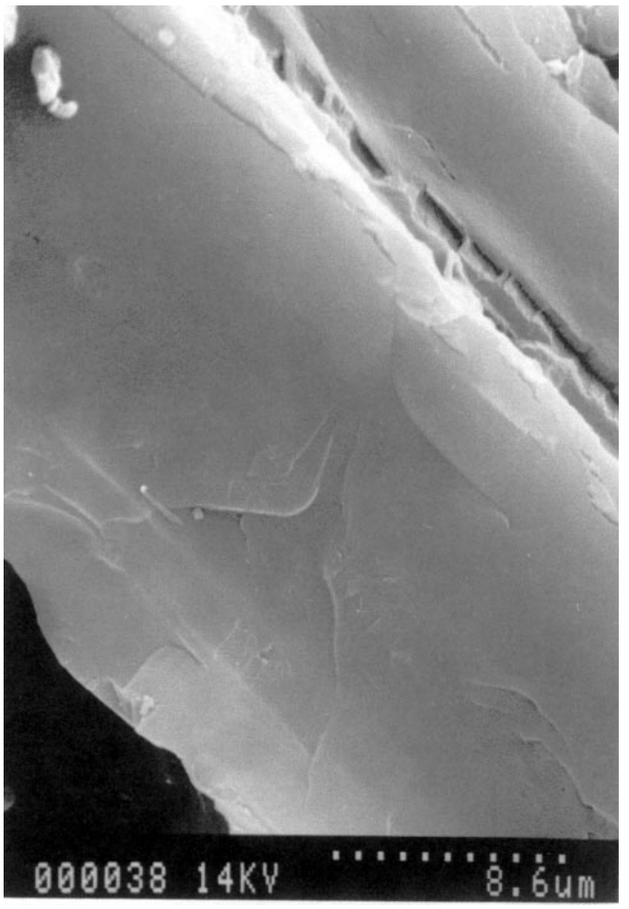

Fig. 8 SEM image of a surface of a raw gel dried at 372 K.

coatings for the preparation of thin films. At 473 K, the temperature was already high enough to initiate a change in the original structure of the gel. Along with increased temperature the gel surface shrinks further and results in the formation of small clusters, which are less than 700 nm in diameter. The size of clusters of the gel after the SFE process was found to be between 450 and 550 nm.

Conclusion

Titania nanosized particles were prepared within templates (reverse micelle) of non-ionic surfactant Triton X-100 in cyclohexane by the sol–gel method using titanium(IV) isopropoxide. The water to surfactant ratio R was kept low ($R=1$) to confine the association of the water molecules with the hydrophilic part of the surfactant to the terminal hydroxyl groups. The process of gelling, yielding a transparent material, took about 110 minutes up to the point of visual completion. Formation of a white precipitate indicating the presence of $Ti(OH)_4$, a product of a complete hydrolysis, was not observed. The raw gels were either treated by thermal means, to obtain the photoactive form of TiO_2—anatase, or the organic content was substantially reduced first by supercritical fluid extraction with carbon dioxide and then also calcined to adjust the crystallographic phase structure of the final product. The supercritical fluid extraction did not remove the surfactant completely; however, its content was substantially reduced. After the SFE the gel already exhibits a very high surface area (about $620\pm5\ m^2\ g^{-1}$) and its structure, as shown by XPS, resembles that of anatase. This was achieved without any thermal treatment. In comparison with the direct thermal treatment this combined method provided smaller nanoparticles with higher surface area and narrow pore size distribution. The TiO_2 sample with the developed crystallographic phase structure of anatase had a surface area of $S_{BET}=781\ m^2\ g^{-1}$, a crystallite size $D=3.8$ nm and a pore size distribution peaking at 3.8 nm for the mesoporous contribution and at 0.8 nm for the microporous region was prepared from the extracted gel at 773 K. On the basis of these results we are currently testing the photoactivity of the precursor gel and the final material.

Acknowledgements

Authors wish to thank to Dr Z. Bastl from the J. Heyrovsky Institute of Physical Chemistry, Academy of Sciences of the Czech Republic for performing XPS analyses and for his kind spectra interpretations.

References

1 D. Papoutsi, P. Lianos, Yianoulis and P. Koutsoukos, *Langmuir*, 1994, **10**, 1684.
2 D. Bersani, G. Antonioli, P. P. Lottici and T. Lopez, *J. Non-Cryst. Solids*, 1998, **232**, 175.
3 E. Haro-Poniatowski, R. Rodriguez-Talavera, M. de la Cruz Heredia and O. Cano-Corona, *J. Mater. Res.*, 1994, **9**, 2102.
4 G. Zhao, S. Utsumi, H. Kozuka and T. Yoko, *J. Mater. Sci.*, 1998, **33**, 3655.
5 J. H. Fendler, *Curr. Opin. Colloid Surf. Sci.*, 1996, **1**, 202.
6 T. Lopez, E. Sanchez, P. Bosch, Y. Meas and R. Gomez, *Mater. Chem. Phys.*, 1992, **32**, 141.
7 L. Auvray, *Faraday Discuss. Chem. Soc.*, 1995, **101**, 235.
8 H. Tada and M. Tanaka, *Langmuir*, 1997, **13**, 360.
9 E. Stathatos, P. Lianos, F. DelMonte, D. Levy and D. Tsiourvas, *Langmuir*, 1997, **13**, 4295.
10 E. Pelizzeti, C. Minero, E. Borgarello, L. Tinucci and N. Serpone, *Langmuir*, 1993, **9**, 2995.
11 A. P. Rivera, K. Tanaka and T. Hisanaga, *Appl. Catal. B*, 1993, **3**, 37.
12 N. N. Lichtin and M. Avudaithai, *Res. Chem. Intermed.*, 1994, **20**, 755.
13 B. Ohtani, Y. Ogawa and S. Nishimoto, *J. Phys. Chem.*, 1997, **101**, 3746.
14 J. L. Ferry and W. H. Glaze, *Langmuir*, 1998, **14**, 3551.
15 C. Anderson and A. J. Bard, *J. Phys. Chem.*, 1995, **99**, 9882.
16 Y. Ohko, A. Fujishima and K. Hashimoto, *J. Phys. Chem.*, 1998, **102**, 1724.
17 R. W. Matthews, *J. Phys. Chem.*, 1987, **91**, 3328.
18 D. S. Muggli, K. H. Lowery and J. L. Falconer, *J. Catal.*, 1998, **180**, 111.
19 Y. Ohya, H. Saiki, T. Tanaka and Y. Takahasi, *J. Am. Ceram. Soc.*, 1996, **79**, 825.
20 Q. Xu and M. A. Anderson, *J. Am. Ceram. Soc.*, 1995, **76**, 2095.
21 H. Shin, M. R. De Guire and A. H. Heuer, *J. Appl. Phys.*, 1998, **83**, 3311.
22 C. Suresh, V. Biju, P. Mukundan and K. G. K. Warrier, *Polyhedron*, 1998, **17**, 3131.
23 S. J. Tsai and S. Cheng, *Catal. Today*, 1997, **33**, 227.
24 T. Yoko, L. Hu, H. Kozuka and S. Sakka, *Thin Solid Films*, 1996, **283**, 188.
25 K. Vinodgopal, S. Hotchandani and P. V. Kamat, *J. Phys. Chem.*, 1993, **97**, 9040.
26 K. Terabe, K. Kato, H. Miyazaki, S. Yamaguchi, A. Imai and Y. Iguchi, *J. Mater. Sci.*, 1994, **29**, 1617.
27 E. Pelizzetti, C. Minero, E. Borgarello, L. Tinucci and N. Serpone, *Langmuir*, 1993, **9**, 2995.
28 A. Fernandez, G. Lassaletta, V. M. Jimenez, A. Justo, A. R. Gonzales-Felipe, J. M. Herrmann, H. Tahiri and Y. Ait-Ichou, *Appl. Catal. B*, 1995, **7**, 49.
29 V. Shklover, M. K. Nazeerudddin, S. M. Zakeeruddin, C. Barbe, A. Kay, T. Haibach, W. Steurer, R. Hermann, H. U. Nissen and M. Grätzel, *Chem. Mater.*, 1997, **9**, 430.
30 U. Bach, D. Lupo, P. Comte, J. E. Moser, F. Weissörtel, J. Salbeck, H. Spreitzer and M. Grätzel, *Nature*, 1998, **395**, 583.
31 S. D. Burnside, V. Skhlover, Ch. Barbe, P. Comte, F. Arendse, K. Brooks and M. Grätzel, *Chem. Mater.*, 1998, **10**, 2419.
32 A. Hagfeldt, J. Björksten and M. Grätzel, *J. Phys. Chem.*, 1996, **100**, 8045.
33 Ch. Barbe, F. Arendse, P. Comte, M. Jirousek, F. Lenzmann, V. Skhlover and M. Grätzel, *J. Am. Ceram. Soc.*, 1997, **80**, 3157.
34 L. Kavan, M. Grätzel, S. E. Gilbert, C. Klemenz and H. J. Scheel, *J. Am. Chem. Soc.*, 1996, **118**, 6716.
35 L. Kavan, M. Grätzel, J. Rathousky and A. Zukal, *J. Electrochem. Soc.*, 1996, **143**, 394.
36 S. Peres-Durand, J. Rouviere and C. Guizard, *Colloids Surf. A*, 1995, **98**, 251.
37 G. Puccetti and R. M. Leblanc, *J. Phys. Chem. B*, 1998, **102**, 9002.
38 J. L. Keddie, P. V. Braun and P. Giannelis, *J. Am. Ceram. Soc.*, 1994, **77**, 1592.
39 W. W. So, S. B. Park and S. J. Moon, *J. Mater. Sci. Lett.*, 1998, **17**, 1219.
40 H. Imai, H. Hirashima and K. Awazu, *Thin Solid Films*, 1999, **351**, 91.
41 H. Fujii, M. Ohtaki and K. Eguchi, *J. Am. Chem. Soc.*, 1998, **120**, 6832.
42 J. M. Herrmann, H. Tahiri, Y. Ait-Ichou, G. Lassaletta, A. R. Gonzales-Felipe and A. Fernandez, *Appl. Catal. B*, 1997, **13**, 219.
43 D. M. Zhu, K. I. Feng and Z. A. Schelly, *J. Phys. Chem.*, 1992, **96**, 2382.
44 R. H. Auerbach, K. Dost, D. C. Jones and G. D. Davidson, *Analyst*, 1999, **124**, 1501.
45 S. Kawi and Lai. M. Wai, *Chem. Commun.*, 1998, 1407.
46 S. Kawi and Lai. M. Wai, *CHEMTECH*, 1998, **28**, 26.
47 S. B. Hawthorne, *Anal. Chem.*, 1990, **62**, 633.
48 M. Kane, J. R. Dean, S. M. Hitchen, C. J. Dowle and R. L. Tranter, *Anal. Proc.*, 1993, **30**, 399.
49 D. G. P. A. Breen, J. M. Horner, K. D. Bartle, A. A. Clifford, J. Waters and J. G. Lawrence, *Water Res.*, 1996, **30**, 476.
50 I. Bach and D. J. Cole-Hamilton, *Chem. Commun.*, 1998, 1463.
51 P. G. Jessop, Y. Hsiao, T. Ikariya and R. Novori, *J. Am. Chem. Soc.*, 1996, **118**, 344.
52 O. Kroscher, R. A. Koppel, M. Froba and A. Baiker, *J. Catal.*, 1998, **178**, 284.
53 K. Mitsuda, H. Kimura and T. Murahasi, *J. Mater. Sci.*, 1989, **24**, 413.
54 W. Brown, R. Rymden, J. van Stam, M. Almgren and G. Svensk, *J. Phys. Chem.*, 1989, **93**, 2512.
55 R. Jha and J. C. Ahluwalia, *J. Phys. Chem.*, 1991, **95**, 7782.
56 B. Anderson and G. Olofsson, *J. Chem. Soc., Faraday Trans. 1*, 1988, **84**, 4087.
57 N. Funasaki, S. Hada and S. Neya, *Bull. Chem. Soc. Jpn.*, 1989, **62**, 1725.
58 D. M. Zhu and Z. A. Schelly, *Langmuir*, 1992, **8**, 48.

59 Powder Diffraction File of the JCPDS, International Centre for Diffraction Data, Swathmore, PA, 1998.
60 I. Moriguchi, H. Maeda, Y. Teraoka and S. Kagawa, *J. Am. Chem. Soc.*, 1995, **117**, 1139.
61 M. Anpo, T. Shima, S. Kodama and Y. Kubokawa, *J. Phys. Chem.*, 1987, **91**, 4305.
62 C. Kormann, D. W. Bahnemann and M. R. Hoffmann, *J. Phys. Chem.*, 1988, **92**, 5196.
63 E. P. Barret, L. G. Joyner and P. P. Halenda, *J. Am. Chem. Soc.*, 1951, **73**, 373.
64 J. Medek, *Fuel*, 1977, **56**, 131.
65 M. M. Dubinin, *Chem. Rev.*, 1960, **60**, 235.
66 H. F. Stoeckli, J. P. Houriet, A. Perret and U. Huber, *Characterisation of Porous Solids*, SCI, London, 1979, pp. 31–39.
67 B. McEnaney, *Carbon*, 1988, **26**, 267.